SIAM J. SCI. COMPUT.
Vol. 44, No. 5, pp. A3317–A3340

HAMILTONIAN-PRESERVING DISCONTINUOUS GALERKIN METHODS FOR THE LIOUVILLE EQUATION WITH DISCONTINUOUS POTENTIAL*

BOYANG YE†, SHI JIN‡, YULONG XING§, AND XINGHUI ZHONG†

Abstract. Numerically solving the Liouville equation in classical mechanics with a discontinuous potential often leads to the challenges of how to preserve the Hamiltonian across the potential barrier and a severe time step constraint according to the Courant–Friedrichs–Lewy condition. Motivated by the Hamiltonian-preserving finite volume schemes by Jin and Wen [21], we introduce a Hamiltonian-preserving discontinuous Galerkin (DG) scheme for the Liouville equation with discontinuous potential in this paper. The DG method can be designed with arbitrary order of accuracy and offers many advantages including easy adaptivity, compact stencils, and the ability of handling complicated boundary conditions and interfaces. We propose to carefully design the numerical fluxes of the DG methods to build the behavior of a classical particle at the potential barrier into the numerical scheme, which ensures the continuity of the Hamiltonian across the potential barrier and the correct transmission and reflection condition. Our scheme is proved to be positive and stable in L^1 norm if the positivity-preserving limiter is applied. Numerical examples are provided to illustrate the accuracy and effectiveness of the proposed numerical scheme.

Key words. discontinuous Galerkin method, Liouville equation, Hamiltonian-preserving, discontinuous potential, positivity-preserving limiter

MSC codes. 65M60, 35L45, 70H99

DOI. 10.1137/22M147952X

1. Introduction.

In this paper, we develop and analyze high order Hamiltonian-preserving discontinuous Galerkin (DG) methods for the d-dimensional Liouville equation in classical mechanics

$$f_t + \nabla_{\mathbf{v}} H \cdot \nabla_{\mathbf{x}} f - \nabla_{\mathbf{x}} H \cdot \nabla_{\mathbf{v}} f = 0, \qquad \mathbf{x}, \mathbf{v} \in \mathbb{R}^d, \tag{1.1}$$

where the Hamiltonian H is given by

$$H = \frac{1}{2}|\mathbf{v}|^2 + V(\mathbf{x}) \tag{1.2}$$

and $V(\mathbf{x})$ is the potential. Here $f(t, \mathbf{x}, \mathbf{v})$ is the probability density function of particles at position $\mathbf{x}$, time t, and traveling with velocity $\mathbf{v}$. The Liouville equation (1.1) can be viewed as a different Eulerian formulation of Newton's second law,

$$\frac{d\mathbf{x}}{dt} = \mathbf{v}, \qquad \frac{d\mathbf{v}}{dt} = -\nabla_{\mathbf{x}} V, \tag{1.3}$$

*Submitted to the journal's Methods and Algorithms for Scientific Computing section February 22, 2022; accepted for publication (in revised form) June 27, 2022; published electronically October 17, 2022.

https://doi.org/10.1137/22M147952X

Funding: The second author was partially supported by the NSFC grant 12031013 and by Innovation Program of Shanghai Municipal Education Commission (2021-01-07-00-02-E0087). The Strategic Priority Research Program of Chinese Academy of Sciences (XDA25010404). The third author was partially supported by the NSF grant DMS-1753581. The fourth author was partially supported by the NSFC grant 11871428.

†School of Mathematical Sciences, Zhejiang University, Hangzhou, Zhejiang 310058, People's Republic of China (11935020@zju.edu.cn, zhongxh@zju.edu.cn).

‡School of Mathematical Sciences, Institute of Natural Sciences, MOE-LSC, Shanghai Jiao Tong University, Shanghai, Shanghai 200240, People's Republic of China (shijin-m@sjtu.edu.cn).

§Department of Mathematics, The Ohio State University, Columbus, OH 43210 USA (xing.205@osu.edu).

which is a Hamiltonian system with the Hamiltonian H defined in (1.2).

If the potential $V(x)$ is smooth, the Liouville equation (1.1) is a linear kinetic equation, which has been well studied in the literature. Many existing numerical methods can be applied to provide good numerical approximation. However, a discontinuous potential $V(x)$ may cause extra challenges both theoretically and numerically, and special attention shall be paid to the case with a potential barrier when the potential $V(x)$ is discontinuous. Potential barriers appear in many practical physical problems including the quantum tunneling, materials or media with interfaces, etc.. Under such a case, the Hamiltonian system (1.3) is a system of ODEs with a measured-valued right-hand side that is not Lipschitz continuous (breaking the assumption which the classical well-posedness theory relies on), nor has a bounded variation (for which the renormalized solution was introduced in [12, 1]). We also refer readers to [3, 28, 2, 16, 27] for more theoretical analysis on the uniqueness of weak solutions to transport equations with discontinuous coefficients. Numerically, standard numerical methods may suffer from two challenges [19]. First, numerical approximation of V_x near the discontinuity is of the order $O(1/\Delta x)$; therefore, if an explicit numerical method is used for time discretization, the stringent Courant–Friedrichs–Lewy (CFL) condition $\Delta t = O(\Delta x \Delta v)$ is required, with Δx, Δv being the mesh size under the one-dimensional spatial space and one-dimensional velocity space (1D1V) setting. This leads to smaller Δt, hence more expensive computation. Second, the Hamiltonian $H = \xi^2/2 + V(x)$ is not preserved across the discontinuities of $V(x)$, which may lead to at least a poor numerical resolution or, more seriously, unphysical solutions [21].

It is well known from classical mechanics that, across a potential barrier, the Hamiltonian should remain constant. Motivated by this, Hamiltonian-preserving methods have been proposed and studied in [19] to solve the Liouville equation with discontinuous potential based on finite difference and finite volume approaches. The main idea was to use the behavior of the classical particle at the potential barrier, namely, transmission or reflection, and build it into the design of the Hamiltonian-preserving methods to be consistent with the constant Hamiltonian across the discontinuity. This mechanism was first used to construct the numerical flux and to build the well-balanced kinetic scheme in [26] for the shallow water equations with nonflat topography in order to preserve the steady state solution. It was also shown in [19] that the proposed explicit Hamiltonian-preserving schemes admit a standard CFL condition $\Delta t = O(\Delta x,\ \Delta v)$, and the positivity property and the stability in L^1 and L^∞ norms are also provided. The proof of the L^1 stability and error estimates of the proposed schemes are further discussed in [34, 35, 33, 23]. We also refer readers to [20, 21] for the Hamiltonian-preserving methods to solve the Liouville equation (1.1) arising from the applications in geometrical optics, with the Hamiltonian $H = c(\mathbf{x})|\mathbf{v}|$, where $c(\mathbf{x})$ is the local wave speed of the medium. It can be viewed as the high frequency limit of the second order wave equation

$$u_{tt} - c(\mathbf{x})^2 \Delta u = 0, \qquad t > 0,\ \mathbf{x} \in \mathbb{R}^d.$$

Here the wave speed $c(\mathbf{x})$ has isolated discontinuities due to different media, and waves crossing the discontinuous interface will be transmitted or reflected. Hamiltonian-preserving methods for more complex cases like high frequency waves propagating through different media can be found in [17, 22, 32].

In this paper, we consider solving the Liouville equation (1.1) in the DG framework. DG methods are a class of finite element methods, where both the numerical solution and the test functions belong to discontinuous piecewise polynomial spaces.

They were first designed to solve linear transport equations in [30] and later were extended to solve hyperbolic conservation laws in a series of papers [7, 8, 9, 10]. DG methods have been successfully applied to a wide range of mathematical models, including the kinetic equations; see [6, 13, 15, 29, 4, 5] and the references therein for an incomplete list.

DG methods enjoy many advantages, including h-p adaptivity, arbitrarily unstructured meshes, compact stencils, efficient parallel implementation, and the ability of handling complicated boundary conditions and curved interface, etc.. The goal of this paper is to design Hamiltonian-preserving DG (HPDG) methods for the Liouville equation (1.1), extending the low order Hamiltonian-preserving finite difference and finite volume methods in [19] to high order HPDG methods. As illustrated in [19], one of the key ideas to design Hamiltonian-preserving methods is to build the behavior of a classical particle at the potential barrier into the numerical scheme. Here, we propose to carefully design the numerical fluxes of the DG methods to adopt such a mechanism. The HPDG method is built upon the standard DG method for hyperbolic conservation laws, with extra attention paid to the design of numerical fluxes at the positions where the potential $V(x)$ is discontinuous to ensure the continuity of the Hamiltonian across the potential barrier. As a result, the boundary integration of numerical fluxes at the cell interfaces may be converted into another integration over a range of cell interfaces, which can be evaluated numerically via a carefully designed Gaussian quadrature rule. In [19, 35], the low order Hamiltonian-preserving finite difference and finite volume methods were proven to be positive and stable in L^1 and L^∞ norm. After extending these to arbitrary high order HPDG methods, one nontrivial challenge lies in the stability of the resulting method. To provide extra robustness and stability, a simple positivity-preserving limiter, studied in [36] for DG methods, is combined with the proposed HPDG methods. We demonstrate theoretically that the resulting DG methods preserve the nonnegativity of the numerical solution and have the L^1 stability, even under the situation when the potential $V(x)$ is discontinuous. Numerical examples are provided for Liouville equations in both 1D1V and two-dimensional spatial space and two-dimensional velocity space (2D2V) settings to demonstrate.

The paper is organized as follows: In section 2, we first discuss the problems with the standard DG method to solve the Liouville equation under 1D1V setting with discontinuous potentials. We then present the Hamiltonian-preserving numerical fluxes by adopting the behavior of classical particles at a potential barrier. This leads to the HPDG methods. In addition, we combine the resulting method with a simple positivity-preserving limiter to ensure the solution stay nonnegative during the simulation. In section 3, we establish the positivity and stability analysis for our Hamiltonian-preserving scheme. We extend the proposed methods to two-dimensional space in section 4. In section 5, several numerical examples are presented to investigate the accuracy and effectiveness of our Hamiltonian-preserving scheme. We conclude the paper with some remarks in section 6.

2. HPDG methods. In this section, we lay out the details of the algorithm formulation of the HPDG method for the Liouville equation (1.1) under the 1D1V setting, given by

$$f_t + \xi f_x - V_x f_\xi = 0, \tag{2.1}$$

equipped with suitable initial and boundary conditions, where ξ denotes the one-dimensional variable in the **v**-direction. Our starting point is the standard DG method

presented in the following section.

2.1. Standard DG methods. In this section, we briefly present the standard DG method for solving (2.1) and discuss the difficulties arising from the discontinuous potentials.

We first introduce some notations. Assume $x \in [-L, L]$ and $\xi \in [-A_c, A_c]$. The domain is uniformly (to simplify the presentation) partitioned as follows:

$$-L = x_{\frac{1}{2}} < x_{\frac{3}{2}} < \cdots < x_{N_x+\frac{1}{2}} = L, \quad -A_c = \xi_{\frac{1}{2}} < \xi_{\frac{3}{2}} < \cdots < \xi_{N_\xi+\frac{1}{2}} = A_c.$$

We use a mesh that is a tensor product of grids in the x- and ξ- direction, respectively, defined as

$$K_{ij} = [x_{i-\frac{1}{2}}, x_{i+\frac{1}{2}}] \times [\xi_{j-\frac{1}{2}}, \xi_{j+\frac{1}{2}}], \quad I_i = [x_{i-\frac{1}{2}}, x_{i+\frac{1}{2}}], \quad J_j = [\xi_{j-\frac{1}{2}}, \xi_{j+\frac{1}{2}}].$$

Denote the cell center as $x_i = \frac{1}{2}(x_{i+\frac{1}{2}} + x_{i-\frac{1}{2}})$ and $\xi_j = \frac{1}{2}(\xi_{j+\frac{1}{2}} + \xi_{j-\frac{1}{2}})$. Denote the mesh size as $\Delta x = x_{i+\frac{1}{2}} - x_{i-\frac{1}{2}}$ and $\Delta\xi = \xi_{j+\frac{1}{2}} - \xi_{j-\frac{1}{2}}$. We also define a DG finite element approximation space as

$$\mathbb{V}_h^k := \{v : v|_{K_{ij}} \in P^k(K_{ij}), \ \ 1 \le i \le N_x, \ 1 \le j \le N_\xi\},$$

where $P^k(K_{ij})$ denotes the set of polynomials of total degree up to k on cell K_{ij}. Denote v^-, v^+ as the left and right limits of the function v at the cell interface, respectively. We also introduce the following notations to simplify the presentation:

$$(u, v)_{K_{ij}} = \int_{K_{ij}} uv \, dxd\xi, \quad \langle u, v\rangle_{I_i} = \int_{I_i} uv \, dx, \quad \langle u, v\rangle_{J_j} = \int_{J_j} uv \, d\xi. \tag{2.2}$$

With a slight abuse of notations, the standard semidiscrete DG method for solving (2.1) is defined as follows: to find a unique function $f : [0, T] \to \mathbb{V}_h^k$ such that, for $i = 1, \ldots, N_x, \ j = 1, \ldots, N_\xi$,

$$\begin{aligned}(f_t, \phi)_{K_{ij}} - (\xi f, \phi_x)_{K_{ij}} + \left\langle \xi \hat{f}_{i+\frac{1}{2},\xi}, \phi(x^-_{i+\frac{1}{2}}, \xi)\right\rangle_{J_j} - \left\langle \xi \hat{f}_{i-\frac{1}{2},\xi}, \phi(x^+_{i-\frac{1}{2}}, \xi)\right\rangle_{J_j} \\ + (V_x f, \phi_\xi)_{K_{ij}} - \left\langle V_x \tilde{f}_{x,j+\frac{1}{2}}, \phi(x, \xi^-_{j+\frac{1}{2}})\right\rangle_{I_i} + \left\langle V_x \tilde{f}_{x,j-\frac{1}{2}}, \phi(x, \xi^+_{j-\frac{1}{2}})\right\rangle_{I_i} = 0\end{aligned} \tag{2.3}$$

holds for all test functions $\phi \in \mathbb{V}_h^k$. Here

$$\hat{f}_{i+\frac{1}{2},\xi} = \hat{f}(x_{i+\frac{1}{2}}, \xi), \qquad \tilde{f}_{x,j+\frac{1}{2}} = \tilde{f}(x, \xi_{j+\frac{1}{2}}) \tag{2.4}$$

are the so-called numerical fluxes, defined at the cell interfaces, and in general depend on the values of the numerical solution f from both sides of the interface. They are usually taken as monotone fluxes, and we refer the readers to the review paper [11] for more details. For example, we can take the following simple upwind numerical fluxes:

$$\hat{f}_{i+\frac{1}{2},\xi} = \begin{cases} f(x^-_{i+\frac{1}{2}}, \xi) & \text{if } \xi \ge 0, \\ f(x^+_{i+\frac{1}{2}}, \xi) & \text{if } \xi < 0, \end{cases} \tag{2.5}$$

$$\tilde{f}_{x,j+\frac{1}{2}} = \begin{cases} f(x, \xi^+_{j+\frac{1}{2}}) & \text{if } V_x \ge 0, \\ f(x, \xi^-_{j+\frac{1}{2}}) & \text{if } V_x < 0. \end{cases} \tag{2.6}$$

Thus we obtain a standard semidiscrete DG scheme for solving the Liouville equation (2.1).

For temporal discretization, we consider the third order strong-stability-preserving (SSP) Runge–Kutta (RK) method [31]. For solving

$$\frac{\mathrm{d}u}{\mathrm{d}t} = \mathcal{L}(u) \tag{2.7}$$

with $\mathcal{L}$ being a spatial discretization operator, the SSP-RK method is given by

$$\begin{aligned} u^{(1)} &= u^n + \Delta t \mathcal{L}(u^n), \\ u^{(2)} &= \frac{3}{4}u^n + \frac{1}{4}\left(u^{(1)} + \Delta t \mathcal{L}(u^{(1)})\right), \\ u^{n+1} &= \frac{1}{3}u^n + \frac{2}{3}\left(u^{(2)} + \Delta t \mathcal{L}(u^{(2)})\right). \end{aligned} \tag{2.8}$$

The standard DG method (2.3), combined with the SSP-RK temporal discretization (2.8), works very well when the potential $V(x)$ is smooth. However, if $V(x)$ contains discontinuity, the standard DG method suffers from the following two difficulties as outlined in [19]:

- The Hamiltonian $H = \xi^2/2 + V(x)$ is not preserved across the discontinuities of $V(x)$, which may lead to an unphysical solution or poor numerical resolution.
- The CFL condition of the DG scheme, coupled with an explicit time discretization, is given by

$$\Delta t \left[\frac{\max_j |\xi_j|}{\Delta x} + \frac{\max_i |V_x|_i}{\Delta \xi}\right] \le CFL, \tag{2.9}$$

  where $|V_x|_i$ denotes some numerical approximation of V_x at $x = x_i$. Usually, to have a stable approximation, the time step needs to satisfy $\Delta t \le O(\Delta x, \Delta \xi)$ for smooth potentials $V(x)$. For discontinuous potential V_x, we have $\max |V_x|_i = O(1/\Delta x)$ in the numerical approximation if one smooths V_x through a few mesh points, which leads to a more stringent and unnecessary CFL condition $\Delta t \le O(\Delta x \Delta \xi)$.

2.2. Hamiltonian-preserving numerical flux. To overcome these numerical difficulties, in this section, we unravel the reconstruction of the Hamiltonian-preserving numerical flux for the DG method for solving the Liouville equation with a discontinuous potential, based on the behavior of a classical particle at a potential barrier.

By the theory of the classical mechanics, a particle at a potential barrier either crosses it with a different momentum or is reflected, depending on its momentum and the strength of the potential barrier. Across the potential barrier, the Hamiltonian $H = \xi^2/2 + V(x)$ should be preserved, i.e.,

$$\frac{1}{2}(\xi^-)^2 + V^- = \frac{1}{2}(\xi^+)^2 + V^+, \tag{2.10}$$

where the superscript $\pm$ denote the right and left limits of the function at the potential barrier. Therefore, at the discontinuity of the potential $V(x)$, given the velocity ξ^- on the left of the discontinuity, the velocity ξ^+ on the right can be computed by this constant Hamiltonian condition, yielding

$$\xi^+ = \begin{cases} \sqrt{(\xi^-)^2 + 2(V^- - V^+)} & \text{if } (\xi^-)^2 + 2(V^- - V^+) \ge 0, \\ -\xi^- & \text{otherwise.} \end{cases} \tag{2.11}$$

More details to explain the behavior of a classical particle at a potential barrier can be found in [19]. We remark here that, in defining numerical fluxes, we use the property that the density function $f(t,x,\xi)$ stays unchanged across the discontinuity of the potential in the following manner:

$$f(t,x^-,\xi^-) = f(t,x^+,\xi^+), \tag{2.12}$$

where x is some discontinuous point of $V(x)$ and $\xi^\pm$ are related by (2.11).

Now we use the above mechanism to construct Hamiltonian-preserving numerical flux of high order DG methods for solving (2.1) in order to maintain a constant Hamiltonian across the potential barrier. Throughout this paper, we assume that the discontinuous points of the potential $V(x)$ are located at the cell interface and that $V(x)$ is Lipschitz continuous in the region between these discontinuities. In order to take care of the discontinuity of the potential, we first introduce numerical fluxes $\hat{f}^+_{i-\frac{1}{2},\xi}, \hat{f}^-_{i+\frac{1}{2},\xi}$ at each cell interface in the x-direction and modify the semidiscrete DG scheme (2.3) as

$$\begin{aligned}(f_t,\phi)_{K_{ij}} - (\xi f,\phi_x)_{K_{ij}} + \left\langle \xi \hat{f}^-_{i+\frac{1}{2},\xi}, \phi(x^-_{i+\frac{1}{2}},\xi)\right\rangle_{J_j} - \left\langle \xi \hat{f}^+_{i-\frac{1}{2},\xi}, \phi(x^+_{i-\frac{1}{2}},\xi)\right\rangle_{J_j} \\ + (V_x f,\phi_\xi)_{K_{ij}} - \left\langle V_x \tilde{f}_{x,j+\frac{1}{2}}, \phi(x,\xi^-_{j+\frac{1}{2}})\right\rangle_{I_i} + \left\langle V_x \tilde{f}_{x,j-\frac{1}{2}}, \phi(x,\xi^+_{j-\frac{1}{2}})\right\rangle_{I_i} = 0,\end{aligned} \tag{2.13}$$

where the numerical fluxes $\tilde{f}_{x,j\pm\frac{1}{2}}$ in the ξ-direction still take the form of upwind fluxes defined in (2.6). Note that, if $V(x)$ is continuous at the point $x_{i-\frac{1}{2}}$, both $\hat{f}^+_{i-\frac{1}{2},\xi}$ and $\hat{f}^-_{i-\frac{1}{2},\xi}$ reduce to the standard numerical fluxes $\hat{f}_{i+\frac{1}{2},\xi}$ as defined earlier.

Now, assume $V(x)$ is discontinuous at $x_{i-\frac{1}{2}}$; our focus is on the reconstruction of the numerical fluxes $\hat{f}^\pm_{i-\frac{1}{2},\xi}$ in the scheme (2.13), which is explained in details in the following.

If $\xi > 0$, following the idea of upwind flux, we define

$$\hat{f}^-_{i-\frac{1}{2},\xi} = f(x^-_{i-\frac{1}{2}},\xi), \tag{2.14}$$

which is the same as the standard upwind flux in (2.5), and ξ is taken from the interior of the cell. But for the other flux $\hat{f}^+_{i-1/2,\xi}$, we define it as

$$\hat{f}^+_{i-\frac{1}{2},\xi} = f(x^-_{i-\frac{1}{2}},\tilde{\xi}), \tag{2.15}$$

where $\tilde{\xi}$ is connected to ξ via the relation (2.10), i.e.,

$$\frac{1}{2}\tilde{\xi}^2 + V(x^-_{i-\frac{1}{2}}) = \frac{1}{2}\xi^2 + V(x^+_{i-\frac{1}{2}}), \tag{2.16}$$

or the equivalent form (2.11):

$$\tilde{\xi} = \begin{cases} \sqrt{\xi^2 - 2(V(x^-_{i-\frac{1}{2}}) - V(x^+_{i-\frac{1}{2}}))} & \text{if } \xi^2 - 2(V(x^-_{i-\frac{1}{2}}) - V(x^+_{i-\frac{1}{2}})) \geq 0, \\ -\xi & \text{otherwise.}\end{cases} \tag{2.17}$$

The definition of the flux (2.15) is consistent with the upwind flux (2.5) when $V(x)$ is continuous since $V(x^-_{i-\frac{1}{2}}) = V(x^+_{i-\frac{1}{2}})$ under such case and we have $\tilde{\xi} = \xi$.

If $\xi < 0$, we similarly define

$$\hat{f}^{+}_{i-\frac{1}{2},\xi} = f(x^{+}_{i-\frac{1}{2}}, \xi), \tag{2.18}$$

following the upwind flux (2.5), and

$$\hat{f}^{-}_{i-\frac{1}{2},\xi} = f(x^{+}_{i-\frac{1}{2}}, \tilde{\xi}), \tag{2.19}$$

where $\tilde{\xi}$ is again connected to ξ via the relation (2.10) or (2.11), i.e.,

$$\tilde{\xi} = \begin{cases} -\sqrt{\xi^2 + 2(V(x^{-}_{i-\frac{1}{2}}) - V(x^{+}_{i-\frac{1}{2}}))} & \text{if } \xi^2 + 2(V(x^{-}_{i-\frac{1}{2}}) - V(x^{+}_{i-\frac{1}{2}})) \geq 0, \\ -\xi & \text{otherwise .} \end{cases} \tag{2.20}$$

Up to now, we have defined the semidiscrete HPDG scheme (2.13) with fluxes discussed in (2.14)–(2.20). The integral of the numerical flux $\tilde{f}_{x,j+\frac{1}{2}}$ in the cell I_i in the scheme (2.13) is in general evaluated by directly applying standard Gaussian quadrature rules in this cell. However, this approach may be inaccurate when dealing with the integral of the Hamiltonian-preserving numerical fluxes $\hat{f}^{\pm}_{i-\frac{1}{2},\xi}$ in the same way since the range of $\tilde{\xi}$ defined in (2.17) and (2.20) with $\xi \in J_j$ may span over more than one cell. Therefore, we have to be more careful when approximating the integrals involving fluxes $\hat{f}^{\pm}_{i-\frac{1}{2},\xi}$.

We now use the case of $\xi > 0$ to explain in details the approximation of these integrals. Here we assume $V(x)$ has a discontinuity at the cell interface $x_{i-\frac{1}{2}}$ with the jump $D = V^{-}_{i-\frac{1}{2}} - V^{+}_{i-\frac{1}{2}} > 0$. The other cases, namely, $D < 0$ or $\xi < 0$, can be treated in a similar fashion. To simplify the presentation, we assume that the mesh in ξ-direction is partitioned such that 0, $\pm\sqrt{2D}$ are located at the cell interface. For the integral $\langle \xi \hat{f}^{-}_{i+\frac{1}{2},\xi}, \phi(x^{-}_{i+\frac{1}{2}}, \xi)\rangle_{J_j}$, it equals to $\langle \xi f(x^{-}_{i+\frac{1}{2}}, \xi), \phi(x^{-}_{i+\frac{1}{2}}, \xi)\rangle_{J_j}$ following the definition (2.14) and thus can be approximated by the standard Gaussian quadrature rules in the cell J_j. The integral $\langle \xi \hat{f}^{+}_{i-\frac{1}{2},\xi}, \phi(x^{+}_{i-\frac{1}{2}}, \xi)\rangle_{J_j}$ is more complicated, and the detailed approximation is given in the following with two cases considered.

If $D = V^{-}_{i-\frac{1}{2}} - V^{+}_{i-\frac{1}{2}} > 0$ and $\xi_{j-\frac{1}{2}} \geq \sqrt{2D}$, with the definition (2.15) and (2.17), we have

$$\begin{aligned} \left\langle \xi \hat{f}^{+}_{i-\frac{1}{2},\xi}, \phi(x^{+}_{i-\frac{1}{2}}, \xi) \right\rangle_{J_j} &= \int_{\xi_{j-\frac{1}{2}}}^{\xi_{j+\frac{1}{2}}} \xi f(x^{-}_{i-\frac{1}{2}}, \tilde{\xi}) \phi(x^{+}_{i-\frac{1}{2}}, \xi) d\xi \\ &= \int_{\eta_{j-\frac{1}{2}}}^{\eta_{j+\frac{1}{2}}} \eta f(x^{-}_{i-\frac{1}{2}}, \eta) \phi\left(x^{+}_{i-\frac{1}{2}}, \sqrt{\eta^2 + 2D}\right) d\eta, \end{aligned} \tag{2.21}$$

where $\eta = \sqrt{\xi^2 - 2D}$ and $\eta_{j\pm\frac{1}{2}} = \sqrt{\xi^2_{j\pm\frac{1}{2}} - 2D}$. There are two possibilities for the locations of two end points $\eta_{j\pm\frac{1}{2}}$, though they may not be at the cell interface any more. They either fall into the same computational cell or belong to different cells. In the former case, the integral (2.21) can be approximated by standard Gaussian quadrature rules with sufficient accuracy. In the latter case, the integral can be approximated by a composite quadrature rule, where we first decompose the integration domain into the union of computational cells (or part of the computational cell near the end point) and then apply standard Gaussian quadrature rules with sufficient accuracy.

If $D = V^-_{i-\frac{1}{2}} - V^+_{i-\frac{1}{2}} > 0$ and $\xi_{j-\frac{1}{2}} < \sqrt{2D}$, it leads to that $\xi_{j+\frac{1}{2}} \le \sqrt{2D}$ due to the assumption that $\sqrt{2D}$ is located at the cell interface. With the definition (2.15) and (2.17), we have

$$\begin{aligned}\left\langle \xi \hat{f}^+_{i-\frac{1}{2},\xi}, \phi(x^+_{i-\frac{1}{2}}, \xi) \right\rangle_{J_j} &= \int_{\xi_{j-\frac{1}{2}}}^{\xi_{j+\frac{1}{2}}} \xi f(x^-_{i-\frac{1}{2}}, \tilde{\xi}) \phi(x^+_{i-\frac{1}{2}}, \xi) d\xi \\ &= \int_{\xi_{j-\frac{1}{2}}}^{\xi_{j+\frac{1}{2}}} \xi f(x^-_{i-\frac{1}{2}}, -\xi) \phi(x^+_{i-\frac{1}{2}}, \xi) d\xi,\end{aligned}$$

which can be approximated by standard Gaussian quadrature rules with sufficient accuracy.

2.3. Positivity-preserving limiter. In this section, we apply a positivity-preserving limiter to the HPDG scheme to provide an extra stabilizing mechanism since the exact solution of the Liouville equation is always nonnegative if the initial condition satisfies this.

Starting from the numerical solution f^n at time level n (for the initial condition, f^0 is simply taken as the standard L^2 projection of the analytical initial condition into $\mathbb{V}_h^k$), a positivity-preserving limiter can be applied to "limit" f^n to obtain a new function $f^{n,new}$, which preserves certain positive properties. The "limited" $f^{n,new}$ is then advanced to the next time level with the SSP-RK time discretization methods (2.8). We present the limiting procedure to compute $f^{n,new}$ from f^n in the following and omit the superscript n for simplicity.

Denote $f_{ij}(x,\xi)$ as the DG approximation polynomial on the cell $K_{i,j}$ and $\bar{f}_{ij}$ as the cell average of $f_{ij}(x,\xi)$ on the cell K_{ij}. The "limited" function f^{new} is defined by

$$f^{new}_{ij}(x,\xi) = \theta_1(f_{ij}(x,\xi) - \bar{f}_{ij}) + \bar{f}_{ij}, \tag{2.22}$$

where $\theta_1 \in [0,1]$ is determined by

$$\theta_1 = \min\left\{ \frac{\bar{f}_{ij}}{\bar{f}_{ij} - f_{\min}}, 1 \right\}, \quad f_{\min} = \min_{(x,\xi)\in K_{ij}} f_{ij}(x,\xi). \tag{2.23}$$

Clearly the cell average of $f^{new}_{ij}(x,\xi)$ over K_{ij} is still $\bar{f}_{ij}$ and $f^{new}_{ij}(x,\xi) \ge 0$ in the cell K_{ij} if $\bar{f}_{ij} \ge 0$. It is worth mentioning that the "limited" function f^{new}_{ij} maintains the order of accuracy of the original DG polynomial f_{ij}. We refer readers to [25, 24, 37, 36] and the references cited therein for more detailed discussions on the positive-preserving and maximum-principle-satisfying limiter.

Remark 2.1. In order to successfully apply the positivity-preserving limiter (2.22), one needs the assumption that $\bar{f}_{ij} \ge 0$. We will analytically prove that the cell average of the DG numerical solution at the next time level t^{n+1} satisfies this assumption in Theorem 3.3.

Remark 2.2. For numerical implementation, the exact value $f_{\min}$ in (2.23) can be easily found for $k = 1, 2$ by comparing a finite set of special points. However, the exact value of $f_{\min}$ is difficult to compute for higher order polynomials ($k > 2$), especially for multidimensional cases. One practical approach is to use $\min_{(x,\xi)\in G} f_{ij}(x,\xi)$ as an approximation, where the set G contains the Gauss–Lobatto quadrature points inside each computational cell and all the quadrature points used to evaluate the integrals in (2.21). As a result of this, the "limited" function f^{new} is no longer positive

everywhere; instead we have $f^{new}(x,\xi) \geq 0$ for any $(x,\xi) \in G$. Note that Theorem 3.3 still holds for such case since the integrals in (3.11) are nonnegative after applying a (composite) quadrature rule based on the points in G.

Remark 2.3. The positivity-preserving limiter (2.22) can be easily extended to be a bound-preserving limiter to enforce the "limited" function $f^{new} \in [0,1]$ and ensure extra stability if the initial condition satisfies it, following the maximum-principle-satisfying limiter in [36]. If the potential $V(x)$ is smooth, it can be analytically proved that the numerical solutions of the DG methods coupling with the bound-preserving limiter stay within the range of $[0,1]$, as done in [36]. When the potential $V(x)$ is discontinuous, the first order finite volume Hamiltonian-preserving method in [19] is shown to be L^∞ stable, and the L^∞ norm is shown to grow with an amplification factor of order $1 + O(\Delta t)$. Thus the bound-preserving property is not clear for the finite volume method which is equivalent with the DG methods of $k = 0$. Therefore we do not engage in depth the bound-preserving property for the high order HPDG methods. We numerically apply the bound-preserving limiter to test its performances in Examples 5.2 and 5.3.

3. Positivity and L^1 stability. In this section, we investigate the positivity-preserving property and L^1 stability of the proposed DG scheme in section 2 for solving the Liouville equation (2.1) with discontinuous potential. The study is based on the simple first order Euler forward temporal discretization. High order SSP-RK time discretizations will keep the validity of the properties since they can be written as convex combinations of forward Euler steps.

A fully discrete scheme for the semidiscrete scheme (2.13) with Euler forward is given by

(3.1)
$$\begin{aligned}\left(\frac{f^{n+1}-f}{\Delta t},\phi\right)_{K_{ij}} &- (\xi f,\phi_x)_{K_{ij}} + \left\langle \xi \hat{f}^-_{i+\frac{1}{2},\xi}, \phi(x^-_{i+\frac{1}{2}},\xi)\right\rangle_{J_j} - \left\langle \xi \hat{f}^+_{i-\frac{1}{2},\xi}, \phi(x^+_{i-\frac{1}{2}},\xi)\right\rangle_{J_j} \\ &+ (V_x f,\phi_\xi)_{K_{ij}} - \left\langle V_x \tilde{f}_{x,j+\frac{1}{2}}, \phi(x,\xi^-_{j+\frac{1}{2}})\right\rangle_{I_i} \\ &+ \left\langle V_x \tilde{f}_{x,j-\frac{1}{2}}, \phi(x,\xi^+_{j-\frac{1}{2}})\right\rangle_{I_i} = 0,\end{aligned}$$

where we omit the superscript of $f^{n,new}$ and still use f to denote the limited solution by the positivity-preserving limiter discussed in section (2.3) at time level n. Here $\tilde{f}_{x,j+\frac{1}{2}}$ are the upwind fluxes defined in (2.6). $\hat{f}^{\pm}_{i+\frac{1}{2},\xi}$ are the the Hamiltonian-preserving fluxes defined in section 2.2 at the discontinuity point $x_{i+\frac{1}{2}}$ of $V(x)$, while $\hat{f}^+_{i+\frac{1}{2},\xi} = \hat{f}^-_{i+\frac{1}{2},\xi} = \hat{f}_{i+\frac{1}{2},\xi}$ are defined in (2.5) for the smooth point $x_{i+\frac{1}{2}}$ of $V(x)$.

The first order version of the proposed DG methods (with polynomial degree $k = 0$) reduces to the finite volume methods designed in [19], and the positivity-preserving limiter (2.22) is not active. Therefore, this first order method has the properties of being positive, L^1 contracting and L^∞ stable as studied in [19]. Next, we would like to prove that some properties also hold for the high order DG methods with polynomials of arbitrary degree. We first show in the following lemma that the one-dimensional integral at the cell boundary is bounded by the cell average.

LEMMA 3.1. *For any $\varphi(x,\xi) \in \mathbb{P}^k(K_{ij})$ and $\varphi(x,\xi) \geq 0$, there exists a positive constant $\omega = \omega(k)$ depending on the polynomial degree k such that*

$$\int_{J_j} \varphi(x^+_{i-\frac{1}{2}},\xi)d\xi \le \frac{\omega}{\Delta x}\overline{(\varphi)}_{K_{ij}}, \qquad \int_{J_j} \varphi(x^-_{i+\frac{1}{2}},\xi)d\xi \le \frac{\omega}{\Delta x}\overline{(\varphi)}_{K_{ij}}, \tag{3.2}$$

$$\int_{I_i} \varphi(x,\xi^-_{j-\frac{1}{2}})dx \le \frac{\omega}{\Delta \xi}\overline{(\varphi)}_{K_{ij}}, \qquad \int_{I_i} \varphi(x,\xi^+_{j-\frac{1}{2}})dx \le \frac{\omega}{\Delta \xi}\overline{(\varphi)}_{K_{ij}}, \tag{3.3}$$

where $\overline{(\varphi)}_{K_{ij}}$ *denotes the integral of* $\varphi(x,\xi)$ *on the cell* K_{ij}.

Proof. Denote $\{\zeta_\ell\}_{\ell=0}^k$ as the Legendre–Gauss–Lobatto quadrature points in $[-1,1]$ and $\{\omega_\ell\}_{\ell=0}^k$ as the associated quadrature weights. By the Legendre–Gauss–Lobatto quadrature rule with $k+1$ points which is exact for polynomials of degree up to $2k-1$, we have

$$\begin{aligned}\overline{(\varphi)}_{K_{ij}} &= \int_{J_j}\int_{I_i} \varphi(x,\xi)dxd\xi = \sum_{\ell=0}^{k} \omega_\ell \Delta x \int_{J_j} \varphi\left(x_i + \frac{\Delta x}{2}\zeta_\ell, \xi\right) d\xi \\ &\ge \omega_0 \Delta x \int_{J_j} \varphi(x_{i-\frac{1}{2}},\xi)d\xi + \omega_k \Delta x \int_{J_j} \varphi(x_{i+\frac{1}{2}},\xi)d\xi,\end{aligned} \tag{3.4}$$

where the last inequality is based on the fact that $\varphi(x,\xi) \ge 0$ and $\omega_\ell > 0$ for $\ell = 0,\dots,k$. Since $\omega_0 = \omega_k$, we obtain (3.2) by setting $\omega = 1/\omega_0$. (3.3) can be proved similarly. ∎

Remark 3.2. The proof is valid for $k > 0$. In particular, $\omega = 2$ when $k = 1$ and $\omega = 6$ when $k = 2$, according to the quadrature weights. For the case when $k = 0$, (3.2) and (3.3) hold with $\omega = 1$ since $\varphi(x,\xi)$ is a constant function with $k = 0$.

Next we investigate the positivity of the fully discrete scheme (3.1). We show in the following theorem that, by adding a positivity-preserving limiter discussed in section 2.3 to the HPDG methods and by coupling with the time evolution by Euler forward method, the resulting Hamiltonian-preserving scheme (3.1) preserves the positivity in the sense that the cell averages are always positive if they are positive initially under suitable CFL conditions. We remark here that the proof cannot be trivially extended from the classical DG methods for hyperbolic conservation laws in [36, 24] due to the complication appeared when the potential $V(x)$ is discontinuous.

THEOREM 3.3 (positivity). *The solution* f^{n+1} *of* (3.1) *satisfies* $\overline{(f^{n+1})}_{K_{ij}} \ge 0$ *under the CFL condition*

$$\omega\Delta t\left(\frac{\max|\xi|}{\Delta x} + \frac{\max_i \sup_{x\in \mathrm{int}(I_i)}|V_x|}{\Delta\xi}\right) \le 1, \tag{3.5}$$

where ω *is the positive constant presented in Lemma* 3.1 *and* $\mathrm{int}(I_m)$ *denotes the interior of the cell* I_m.

Proof. For simplicity, we again assume that the mesh in ξ-direction is partitioned such that 0, $\pm\sqrt{2D}$ are located at cell interfaces. We consider the case when $\xi > 0$, $V(x)$ has only one discontinuity point located at the cell interface $x_{m-\frac{1}{2}}$ with jump $D = V^-_{m-\frac{1}{2}} - V^+_{m-\frac{1}{2}} > 0$, and $V'(x) < 0$ at smooth points. The other cases, namely, when $\xi < 0$ or the potential $V(x)$ has several discontinuity points with positive or negative jumps, or $V'(x) > 0$, can be discussed in the similar fashion.

The fully discrete scheme (3.1) with the test function taken as $\phi \equiv 1$ yields

$$\frac{\overline{(f^{n+1})}_{K_{ij}} - \overline{(f)}_{K_{ij}}}{\Delta t} + \left\langle \xi \hat{f}^-_{i+\frac{1}{2},\xi}\right\rangle_{J_j} - \left\langle \xi \hat{f}^+_{i-\frac{1}{2},\xi}\right\rangle_{J_j} - \left\langle V_x \tilde{f}_{x,j+\frac{1}{2}}\right\rangle_{I_i} + \left\langle V_x \tilde{f}_{x,j-\frac{1}{2}}\right\rangle_{I_i} = 0. \tag{3.6}$$

Here f is the limited solution at time level n after applying the positivity-preserving limiter, and thus $f(x,\xi) \geq 0, (x,\xi) \in K_{ij}$ for $i = 1, \ldots, N_x$, $j = 1, \ldots, N_\xi$.

Recall that the discontinuity of $V(x)$ is located at $x_{m-\frac{1}{2}}$, and $\sqrt{2D}$ is a grid point in the ξ-direction. When $i = m$, with the Hamiltonian-preserving fluxes defined in section 2.2, we have

- if $\xi_{j-\frac{1}{2}}^2 - 2D \geq 0$,

$$\frac{\overline{(f^{n+1})}_{K_{mj}} - \overline{(f)}_{K_{mj}}}{\Delta t} + \int_{J_j} \xi f(x^-_{m+\frac{1}{2}}, \xi) d\xi - \int_{\eta_{j-\frac{1}{2}}}^{\eta_{j+\frac{1}{2}}} \eta f(x^-_{m-\frac{1}{2}}, \eta) d\eta - \left\langle V_x \tilde{f}_{x,j+\frac{1}{2}} \right\rangle_{I_m} + \left\langle V_x \tilde{f}_{x,j-\frac{1}{2}} \right\rangle_{I_m} = 0, \tag{3.7}$$

  where $\eta = \sqrt{\xi^2 - 2D}$ and $\eta_{j\pm\frac{1}{2}} = \sqrt{\xi_{j\pm\frac{1}{2}}^2 - 2D}$;

- if $\xi_{j-\frac{1}{2}}^2 - 2D < 0$,

$$\frac{\overline{(f^{n+1})}_{K_{mj}} - \overline{(f)}_{K_{mj}}}{\Delta t} + \int_{J_j} \xi f(x^-_{m+\frac{1}{2}}, \xi) d\xi - \int_{J_j} \xi f(x^+_{m-\frac{1}{2}}, -\xi) d\xi - \left\langle V_x \tilde{f}_{x,j+\frac{1}{2}} \right\rangle_{I_m} + \left\langle V_x \tilde{f}_{x,j-\frac{1}{2}} \right\rangle_{I_m} = 0. \tag{3.8}$$

By Lemma 3.1 and (2.6), we have

$$\int_{J_j} \xi f(x^-_{m+\frac{1}{2}}, \xi) d\xi \leq |\xi_{j+\frac{1}{2}}| \int_{J_j} f(x^-_{m+\frac{1}{2}}, \xi) d\xi \leq \frac{\omega |\xi_{j+\frac{1}{2}}|}{\Delta x} \overline{(f)}_{K_{mj}}, \tag{3.9}$$

$$- \left\langle V_x \tilde{f}_{x,j+\frac{1}{2}} \right\rangle_{I_m} = - \int_{I_m} V_x f(x, \xi^-_{j+\frac{1}{2}}) dx \leq \frac{\omega \sup_{x \in \mathrm{int}(I_m)} |V_x|}{\Delta \xi} \overline{(f)}_{K_{mj}}, \tag{3.10}$$

where $\mathrm{int}(I_m)$ denotes the interior of the cell I_m, i.e., $\mathrm{int}(I_m) = (x_{m-\frac{1}{2}}, x_{m+\frac{1}{2}})$. Since $V(x)$ is Lipschitz continuous for $x \in \mathrm{int}(I_m)$ under our assumption, $\sup_{x \in \mathrm{int}(I_m)} |V_x|$ has a finite upper bound. Notice that $\eta \geq 0, \eta_{j\pm\frac{1}{2}} \geq 0$, combining with the assumption that $\xi > 0$, $V'(x) < 0$ at smooth points and f being nonnegative, yielding

$$\int_{\eta_{j-\frac{1}{2}}}^{\eta_{j+\frac{1}{2}}} \eta f(x^-_{m-\frac{1}{2}}, \eta) d\eta \geq 0, \qquad \int_{J_j} \xi f(x^+_{m-\frac{1}{2}}, -\xi) d\xi \geq 0 \tag{3.11}$$

and

$$\left\langle V_x \tilde{f}_{x,j-\frac{1}{2}} \right\rangle_{I_i} = \left\langle V_x f(x, \xi^-_{j-\frac{1}{2}}) \right\rangle_{I_i} \leq 0. \tag{3.12}$$

Therefore, we have, by (3.7)–(3.12),

$$\overline{(f)}^{n+1}_{K_{mj}} \geq \left(1 - \omega \Delta t \left(\frac{|\xi_{j+\frac{1}{2}}|}{\Delta x} + \frac{\sup_{x \in \mathrm{int}(I_m)} |V_x|}{\Delta \xi} \right) \right) \overline{(f)}_{K_{mj}}. \tag{3.13}$$

This proves that $\overline{(f)}^{n+1}_{K_{mj}} \geq 0$ under the CFL condition (3.5).

For the case when $i \neq m$, the fully discrete scheme (3.1) is simply the standard DG scheme with upwind fluxes. A similar proof can be found in [37, 36] and thus is omitted. ∎

Remark 3.4. The CFL condition (3.5) in Theorem 3.3 is similar to the CFL condition (2.9). However, $|V_x|$ now represents the derivative of the potential $V(x)$ at its Lipschitz continuous region and thus has an $O(1)$ upper bound since $V(x)$ is only discontinuous at grid points under our assumption. Thus our proposed scheme has a hyperbolic CFL condition.

Now we study the stability property of the proposed scheme.

THEOREM 3.5 (L^1 contracting). *Assume that $f(x,\xi)=0$ at the boundary, and no particles come from outside of the domain $[-L,L]\times[-A_c,A_c]$. Then the solution f^{n+1} of* (3.1) *is L^1 contracting, i.e.,*

$$\sum_{ij}|\overline{(f)^{n+1}}_{K_{ij}}|\le\sum_{ij}|\overline{(f)}_{K_{ij}}| \tag{3.14}$$

under the CFL condition (3.5).

Remark 3.6. Due to the linearity of the scheme (3.1), the equation for the error between the analytical solution and the numerical solution is the same as the scheme (3.1) itself. Thus we assume there is no error at the boundary, and zero Dirichlet boundary conditions can be considered as a simplified case.

Remark 3.7. After applying the positivity-preserving limiter (2.22), the limited numerical solution at time lever $n+1$, i.e., $f^{n+1,new}$, is nonnegative and also maintains the cell average of the solution f^{n+1}. Thus we have $\overline{(|f|)^{n+1,new}}_{K_{ij}}=|\overline{(f)^{n+1,new}}_{K_{ij}}|=|\overline{(f)^{n+1}}_{K_{ij}}|$. Combining with (3.14) leads to

$$\|f^{n+1,new}\|_{L^1}\le\|f^{n,new}\|_{L^1},$$

i.e., the L^1 stability property of the numerical solutions.

Proof. For simplicity, we again consider the case when $V(x)$ has only one discontinuity at the cell interface $x_{m-\frac12}$ with jump $D=V^-_{m-\frac12}-V^+_{m-\frac12}>0$, and $V'(x)<0$ at smooth points. The other cases can be discussed similarly. We again assume that the mesh is partitioned such that $0,\ \pm\sqrt{2D}$ are grid points in ξ-direction. We further assume that $\xi_{N_\xi+\frac12}>\sqrt{2D}$ to include all the possible behaviors of the particles such as crossing the potential barrier with increased/reduced momentum or being reflected.

By taking the test function $\phi\equiv1$ in the fully discrete scheme (3.1), we can rewrite it as

$$\frac{\overline{(f^{n+1})}_{K_{ij}}-\overline{(f)}_{K_{ij}}}{\Delta t}=\underbrace{-\left\langle\xi\hat f^-_{i+\frac12,\xi}\right\rangle_{J_j}+\left\langle\xi\hat f^+_{i-\frac12,\xi}\right\rangle_{J_j}+\left\langle V_x\tilde f_{x,j+\frac12}\right\rangle_{I_i}-\left\langle V_x\tilde f_{x,j-\frac12}\right\rangle_{I_i}}_{R_{ij}}. \tag{3.15}$$

Here f is the limited solution at time level n after applying the positivity-preserving limiter, and thus $f(x,\xi)\ge0,(x,\xi)\in K_{ij}$ for $i=1,\dots,N_x$, $j=1,\dots,N_\xi$. By Theorem (3.3), we have $\overline{(f^{n+1})}_{K_{ij}}\ge0$ under the CFL condition (3.5). Therefore, to show the L^1 contracting property (3.14), we only need to prove that

$$\sum_{ij}R_{ij}\le0.$$

With the upwind fluxes defined in (2.5) and (2.6) and the Hamiltonian-preserving numerical fluxes defined in (2.14), (2.15), (2.18), and (2.19), we have

(1) if $\xi_j > 0$, $i \neq m$,

$$R_{ij} = -\int_{J_j} \xi f(x^-_{i+\frac{1}{2}}, \xi) d\xi + \int_{J_j} \xi f(x^-_{i-\frac{1}{2}}, \xi) d\xi + \left\langle V_x \tilde{f}_{x,j+\frac{1}{2}} \right\rangle_{I_i} - \left\langle V_x \tilde{f}_{x,j-\frac{1}{2}} \right\rangle_{I_i}; \tag{3.16}$$

(2) if $\xi_j < 0$, $i \neq m-1$,

$$R_{ij} = -\int_{J_j} \xi f(x^+_{i+\frac{1}{2}}, \xi) d\xi + \int_{J_j} \xi f(x^+_{i-\frac{1}{2}}, \xi) d\xi + \left\langle V_x \tilde{f}_{x,j+\frac{1}{2}} \right\rangle_{I_i} - \left\langle V_x \tilde{f}_{x,j-\frac{1}{2}} \right\rangle_{I_i}; \tag{3.17}$$

(3) if $\xi_j > 0$, $i = m$,

$$R_{ij} = -\int_{J_j} \xi f(x^-_{i+\frac{1}{2}}, \xi) d\xi + \left\langle \xi \hat{f}^+_{i-\frac{1}{2},\xi} \right\rangle_{J_j} + \left\langle V_x \tilde{f}_{x,j+\frac{1}{2}} \right\rangle_{I_i} - \left\langle V_x \tilde{f}_{x,j-\frac{1}{2}} \right\rangle_{I_i}; \tag{3.18}$$

(4) if $\xi_j < 0$, $i = m-1$,

$$R_{ij} = -\left\langle \xi \hat{f}^-_{i+\frac{1}{2},\xi} \right\rangle_{J_j} + \int_{J_j} \xi f(x^+_{i-\frac{1}{2}}, \xi) d\xi - \left\langle V_x \tilde{f}_{x,j+\frac{1}{2}} \right\rangle_{I_i} + \left\langle V_x \tilde{f}_{x,j-\frac{1}{2}} \right\rangle_{I_i}. \tag{3.19}$$

Summing up (3.16)–(3.19) over all the elements i, j, we have

$$\begin{aligned} \sum_{ij} R_{ij} = &\sum_{\xi_j > 0} \left(\left\langle \xi \hat{f}^+_{m-\frac{1}{2},\xi} \right\rangle_{J_j} - \int_{J_j} \xi f(x^-_{m-\frac{1}{2}}, \xi) d\xi \right) \\ &- \sum_{\xi_j < 0} \left(\left\langle \xi \hat{f}^-_{m-\frac{1}{2},\xi} \right\rangle_{J_j} - \int_{J_j} \xi f(x^+_{m-\frac{1}{2}}, \xi) d\xi \right), \end{aligned} \tag{3.20}$$

due to zero boundary condition, and all the numerical fluxes in the ξ-direction cancel after the summation. To simplify the presentation, we omit the subscript $m - \frac{1}{2}$ in the following. Let us introduce the notations

$$\eta = \sqrt{\xi^2 - 2D}, \quad \eta_{j\pm\frac{1}{2}} = \sqrt{\xi^2_{j\pm\frac{1}{2}} - 2D}, \quad \eta' = -\sqrt{\xi^2 + 2D}, \quad \eta'_{j\pm\frac{1}{2}} = -\sqrt{\xi^2_{j\pm\frac{1}{2}} + 2D}.$$

By a change of variables as in (2.21) and utilizing the definition of the Hamiltonian-preserving numerical fluxes $\hat{f}^{\pm}$ in section 2.2, we obtain

(3.21)

$$\begin{aligned}
\sum_{ij} R_{ij} = & \sum_{\xi_{j-\frac{1}{2}} \geq \sqrt{2D}} \int_{\eta_{j-\frac{1}{2}}}^{\eta_{j+\frac{1}{2}}} \eta f(x^-, \eta) d\eta + \sum_{0 \leq \xi_{j-\frac{1}{2}} < \sqrt{2D}} \int_{J_j} \xi f(x^-, -\xi) d\xi \\
& - \sum_{\xi_j > 0} \int_{J_j} \xi f(x^-, \xi) d\xi + \sum_{\xi_j < 0} \int_{J_j} \xi f(x^+, \xi) d\xi - \sum_{\xi_{j+\frac{1}{2}} \leq 0} \int_{\eta'_{j-\frac{1}{2}}}^{\eta'_{j+\frac{1}{2}}} \eta' f(x^+, \eta') d\eta' \\
= & \int_0^{\sqrt{\xi^2_{N_\xi+\frac{1}{2}} - 2D}} \eta f(x^-, \eta) d\eta - \int_{-\sqrt{2D}}^0 \xi f(x^+, \xi) d\xi \\
& - \int_0^{\xi_{N_\xi+\frac{1}{2}}} \xi f(x^-, \xi) d\xi + \int_{-\xi_{N_\xi+\frac{1}{2}}}^0 \xi f(x^+, \xi) d\xi - \int_{-\sqrt{\xi^2_{N_\xi+\frac{1}{2}} + 2D}}^{-\sqrt{2D}} \eta' f(x^+, \eta') d\eta' \\
= & - \int_{\sqrt{\xi^2_{N_\xi+\frac{1}{2}} - 2D}}^{\xi_{N_\xi+\frac{1}{2}}} \xi f(x^-, \xi) d\xi + \int_{-\sqrt{\xi^2_{N_\xi+\frac{1}{2}} + 2D}}^{-\xi_{N_\xi+\frac{1}{2}}} \xi f(x^+, \xi) d\xi \leq 0,
\end{aligned}$$

where the second equality is due to the fact that 0 and $\pm\sqrt{2D}$ are located at the cell interfaces in the ξ-direction, and the last inequality follows from the fact that f is nonnegative and that no particles come from outside of the domain according to our assumption. ∎

4. Extension to higher dimensions. In this section, we extend our proposed scheme for the Liouville equation under 1D1V setting to higher dimensions. As an example, we consider the Liouville equation

$$f_t + \xi f_x + \eta f_y - V_x f_\xi - V_y f_\eta = 0 \tag{4.1}$$

in the 2D2V setting. Let $\mathcal{T}_h$ be uniform partition of the computational domain with the meshes $K_{ij\kappa\ell} = I_i^{(x)} \times I_j^{(y)} \times J_\kappa^{(\xi)} \times J_\ell^{(\eta)} = [x_{i-\frac{1}{2}}, x_{i+\frac{1}{2}}] \times [y_{j-\frac{1}{2}}, y_{j+\frac{1}{2}}] \times [\xi_{\kappa-\frac{1}{2}}, \xi_{\kappa+\frac{1}{2}}] \times [\eta_{\ell-\frac{1}{2}}, \eta_{\ell+\frac{1}{2}}]$ and the cell interfaces located at $x_{i+\frac{1}{2}}$,$y_{j+\frac{1}{2}}$,$\xi_{\kappa+\frac{1}{2}}$,$\eta_{\ell+\frac{1}{2}}$ in each direction. The mesh size is denoted by $\Delta x = x_{i+\frac{1}{2}} - x_{i-\frac{1}{2}}$, $\Delta y = y_{j+\frac{1}{2}} - y_{j-\frac{1}{2}}$, $\Delta\xi = \xi_{\kappa+\frac{1}{2}} - \xi_{\kappa-\frac{1}{2}}$, $\Delta\eta = \eta_{\ell+\frac{1}{2}} - \eta_{\ell-\frac{1}{2}}$. Let us define a high-dimensional DG finite element approximation space

$$\mathbb{W}_h^k = \{v : v|_{K_{ij\kappa\ell}} \in P^k(K_{ij\kappa\ell}),\ K_{ij\kappa\ell} \in \mathcal{T}_h\}.$$

Similarly to the one-dimensional case, the semidiscrete HPDG scheme for the 2D2V Liouville equation (4.1) is defined as, for any test function $\phi \in \mathbb{W}_h^k$, we have

$$\begin{aligned}
(f_t, \phi)_{K_{ij\kappa\ell}} & - (\xi f, \phi_x)_{K_{ij\kappa\ell}} - (\eta f, \phi_y)_{K_{ij\kappa\ell}} + (V_x f, \phi_\xi)_{K_{ij\kappa\ell}} + (V_y f, \phi_\eta)_{K_{ij\kappa\ell}} \\
& + \left\langle \xi \hat{\hat{f}}^-_{i+\frac{1}{2},j,\xi,\eta}, \phi(x^-_{i+\frac{1}{2}}, y, \xi, \eta) \right\rangle_{I_j^{(y)} \times J_\kappa^{(\xi)} \times J_\ell^{(\eta)}} \\
& - \left\langle \xi \hat{\hat{f}}^+_{i-\frac{1}{2},j,\xi,\eta}, \phi(x^+_{i-\frac{1}{2}}, y, \xi, \eta) \right\rangle_{I_j^{(y)} \times J_\kappa^{(\xi)} \times J_\ell^{(\eta)}} \\
& + \left\langle \eta \hat{\hat{f}}^-_{i,j+\frac{1}{2},\xi,\eta}, \phi(x, y^-_{j+\frac{1}{2}}, \xi, \eta) \right\rangle_{I_i^{(x)} \times J_\kappa^{(\xi)} \times J_\ell^{(\eta)}}
\end{aligned}$$

$$
\begin{aligned}
&- \left\langle \eta \hat{\tilde{f}}^{+}_{i,j-\frac{1}{2},\xi,\eta}, \phi(x, y^{+}_{j-\frac{1}{2}}, \xi, \eta) \right\rangle_{I_i^{(x)} \times J_\kappa^{(\xi)} \times J_\ell^{(\eta)}} \\
&- \left\langle V_x \tilde{\tilde{f}}_{x,y,\kappa+\frac{1}{2},\eta}, \phi(x, y, \xi^{-}_{\kappa+\frac{1}{2}}, \eta) \right\rangle_{I_i^{(x)} \times I_j^{(y)} \times J_\ell^{(\eta)}} \\
&+ \left\langle V_x \tilde{\tilde{f}}_{x,y,\kappa-\frac{1}{2},\eta}, \phi(x, y, \xi^{+}_{\kappa-\frac{1}{2}}, \eta) \right\rangle_{I_i^{(x)} \times I_j^{(y)} \times J_\ell^{(\eta)}} \\
&- \left\langle V_y \tilde{\tilde{f}}_{x,y,\xi,\ell+\frac{1}{2}}, \phi(x, y, \xi, \eta^{-}_{\ell+\frac{1}{2}}) \right\rangle_{I_i^{(x)} \times I_j^{(y)} \times J_\ell^{(\xi)}} \\
&+ \left\langle V_y \tilde{\tilde{f}}_{x,y,\xi,\ell-\frac{1}{2}}, \phi(x, y, \xi, \eta^{+}_{\ell-\frac{1}{2}}) \right\rangle_{I_i^{(x)} \times I_j^{(y)} \times J_\ell^{(\xi)}} \\
&= 0,
\end{aligned}
$$

where numerical fluxes $\tilde{\tilde{f}}$ and $\tilde{\tilde{f}}$ in the ξ- and η-direction take the upwind fluxes as defined in (2.6). We also define the fluxes $\hat{\tilde{f}}^{\pm}$ and $\hat{\tilde{f}}^{\pm}$ at the cell interface to account for the discontinuous potential. They are defined following the same procedure as in section 2.2 to preserve a constant Hamiltonian across the potential barrier. The two-dimensional version of the positivity-preserving limiter, similar to those in (2.22), can be applied to enhance the stability and preserve nonnegativity of density distribution f. The third order SSP-RK temporal discretization (2.8) can again be utilized to advance in time.

5. Numerical results. In this section, we present some numerical tests to demonstrate the performance of the proposed HPDG scheme with the positivity-preserving limiter. In the examples, the time step size is set as $\Delta t = \mathrm{CFL} \cdot \Delta x$, where CFL is taken as indicated in (3.5). For the accuracy tests (e.g., Example 5.1), we adjust the time step Δt as $\Delta t = \mathrm{CFL} \cdot \Delta x^{4/3}$ for the P^3 case so that the temporal and spatial errors are of the same level.

Example 5.1 (accuracy test). In this example, we consider the following Liouville equation in a 1D1V setting

$$
f_t + \xi f_x - V_x f_\xi = S(t, x, \xi) \ , \ (x, \xi) \in [-\pi, \pi] \times [-\pi, \pi] \tag{5.1}
$$

to test the accuracy of the HPDG scheme, where $S(t, x, \xi)$ is the source term. We consider the following two settings.

- **Case I**: The potential $V(x) = -\frac{x^2}{2}$ is continuous, and $S(t, x, \xi) = (x + \xi - 1)\cos(x + \xi - t)$. The exact solution in this case is

$$
f(t, x, \xi) = \sin(x + \xi - t).
$$

- **Case II**: The potential $V(x)$ is discontinuous, given by

$$
V(x) = \begin{cases} 0.5, & x \le 0, \\ 0, & x > 0, \end{cases}
$$

and

$$
S(t, x, \xi) = \begin{cases} (\xi - 1)\cos(x + \sqrt{|\xi^2 - 1|} - t), & x \ge 0, \xi > -1, \\ (\xi - 1)\cos(x - \sqrt{\xi^2 - 1} - t), & x \ge 0, \xi \le -1, \\ (\xi - 1)\cos(x + \xi - t), & \text{otherwise.} \end{cases}
$$

TABLE 5.1
Errors and orders of accuracy for the HPDG method for the Liouville equation with continuous potential in Example 5.1.

	P^1				P^2			
$N_x \times N_\xi$	L^1 error	Order	L^∞ error	Order	L^1 error	Order	L^∞ error	Order
30×30	1.58E-02		1.93E-03		2.71E-04		7.46E-05	
40×40	8.89E-03	2.00	1.08E-03	2.01	1.14E-04	3.00	3.12E-05	3.04
50×50	5.69E-03	2.00	6.88E-04	2.03	5.74E-05	3.09	1.59E-05	3.00
75×75	2.52E-03	2.01	3.04E-04	2.02	1.68E-05	3.03	4.99E-06	2.86
100×100	1.41E-03	2.01	1.71E-04	1.99	7.05E-06	3.02	2.12E-06	2.98

	P^3			
$N_x \times N_\xi$	L^1 error	Order	L^∞ error	Order
30×30	4.82E-06		1.68E-06	
40×40	1.57E-06	3.91	5.07E-07	4.16
50×50	6.19E-07	4.16	2.09E-07	3.97
75×75	1.21E-07	4.02	4.07E-08	4.04
100×100	3.83E-08	4.01	1.27E-08	4.04

The exact solution in this case is

$$f(t,x,\xi) = \begin{cases} \sin(x + \sqrt{|\xi^2 - 1|} - t), & x \geq 0, \xi > -1, \\ \sin(x - \sqrt{\xi^2 - 1} - t), & x \geq 0, \xi \leq -1, \\ \sin(x + \xi - t), & \text{otherwise.} \end{cases}$$

We perform numerical simulations up to $t = 0.1$ using the HPDG method with polynomials of degree k, $k = 1, 2, 3$. For Case I with continuous potential, the L^1 and L^∞ errors and orders of accuracy are listed in Table 5.1. For Case II with discontinuous potential, the errors are measured outside the "pollution domain" near the discontinuities. The pollution domain is taken as

$$\Big\{[-\pi, 0]\times([-\pi, -c_1] \cup [-c_2, 0])\Big\} \cup \Big\{[0, \pi]\times\Big(\Big[-1 - \frac{\pi}{10}, -1 + \frac{\pi}{10}\Big] \cup \Big[1 - \frac{\pi}{10}, 1 + \frac{\pi}{10}\Big]\Big)\Big\},$$

where $c_1 = \sqrt{\xi_{max}^2 - 2D} + \frac{\pi}{10}$ and $c_2 = \sqrt{\xi_c^2 - 2D}$ with $\xi_{max} = \pi, \xi_c = -1 - \frac{\pi}{10}$ and $D = 0.5$. We list the errors and orders of accuracy for Case II in Table 5.2. We can see that, for the Liouville equation (5.1) under the settings of both cases, the HPDG scheme with all three polynomial spaces can achieve the optimal $(k + 1)$th order of accuracy.

Example 5.2 (1D1V problem with an exact L^∞ solution). In this example, we consider one-dimensional Liouville equation (2.1) with a discontinuous potential $V(x)$ given by

$$V(x) = \begin{cases} 0.2, & x < 0, \\ 0, & x > 0, \end{cases} \tag{5.2}$$

and the initial condition set as

$$f(0,x,\xi) = \begin{cases} 1, & x \leq 0, \xi > 0, \sqrt{x^2 + \xi^2} < 1, \\ 1, & x \geq 0, \xi < 0, \sqrt{x^2 + \xi^2} < 1, \\ 0, & \text{otherwise.} \end{cases} \tag{5.3}$$

The computational domain is set as $[-1.5, 1.5] \times [-1.5, 1.5]$. This is a 1D1V problem with an exact L^∞ solution available, and the exact solution at time $t = 1$, as

TABLE 5.2
Errors and orders of accuracy for the HPDG method for the Liouville equation with discontinuous potential in Example 5.1.

	P^1				P^2			
$N_x \times N_\xi$	L^1 error	Order	L^∞ error	Order	L^1 error	Order	L^∞ error	Order
30×30	2.05E-02		7.89E-03		4.24E-04		1.87E-04	
40×40	1.16E-02	1.99	4.69E-03	1.81	1.79E-04	2.99	7.60E-05	3.13
50×50	7.42E-03	1.99	3.06E-03	1.91	9.16E-05	3.01	4.09E-05	2.78
75×75	3.30E-03	2.00	1.40E-03	1.93	2.72E-05	2.99	1.16E-05	3.11
100×100	1.86E-03	1.99	8.10E-04	1.90	1.15E-05	3.00	5.02E-06	2.91

	P^3			
$N_x \times N_\xi$	L^1 error	Order	L^∞ error	Order
30×30	7.09E-06		5.42E-06	
40×40	2.23E-06	4.02	1.42E-06	4.65
50×50	9.09E-07	4.02	5.70E-07	4.09
75×75	1.80E-07	3.99	1.36E-07	3.54
100×100	5.71E-08	4.00	4.25E-08	4.05

constructed in [19], is given by
(5.4)

$$f(1,x,\xi) = \begin{cases} 1, & x \geq 0,\ \ \xi < \sqrt{0.4},\ \ \xi \geq x, \\ 1, & 0 \leq x < 1,\ \ \xi < 0,\ \ \xi > \dfrac{x - \sqrt{2-x^2}}{2}, \\ 1, & x \leq 0,\ \ x < \left(1 - \dfrac{\sqrt{0.6-\xi^2}}{\sqrt{0.4+\xi^2}}\right)\xi,\ \ -\sqrt{0.6} < \xi < x, \\ 1, & -1 < x \leq 0,\ \ \xi > 0,\ \ \xi < \dfrac{x + \sqrt{2-x^2}}{2}, \\ 1, & x \geq 0,\ \ x > \left(1 - \dfrac{\sqrt{1.4-\xi^2}}{\sqrt{\xi^2-0.4}}\right)\xi,\ \ \xi > x, \sqrt{0.4} < \xi < \sqrt{1.4}, \\ 0, & \text{otherwise.} \end{cases}$$

We perform numerical simulations on 100×100 meshes for the proposed DG method with P^2 polynomials up to $t = 1$. Figure 5.1 shows the initial solution (taken as the standard L^2 projection of the initial condition (5.3)), the "limited" initial solution after applying the total variation bounded (TVB) minmod limiter [10] or the bound-preserving limiter to keep $0 \leq f(x,\xi,0) \leq 1$. Figure 5.2 shows the numerical solution at $t = 1$ obtained by the HPDG method only, the numerical solution obtained by the HPDG method with the TVB minmod limiter, and the numerical solution obtained by the HPDG method with the bound-preserving limiter. We observe that there are some oscillations in the plots of the initial condition when projecting the solutions to the piecewise P^2 polynomial space since the initial solution is discontinuous. When either limiter is applied, there are no oscillations in the numerical solutions. For this example, the boundary-preserving limiter can achieve good nonoscillatory results as the TVB minmod limiter, and a sharp and smooth interface can be observed numerically.

We also plot in Figure 5.3(b) the time evolution of $\int f dx d\xi$, which is also the L^1 norm of the numerical solution, since f is nonnegative under the bound-preserving limiter. It can be observed that the L^1 norm of the numerical solution is decreasing as time evolves, which reflects the L^1 contracting property of the HPDG scheme illustrated in Theorem 3.5.

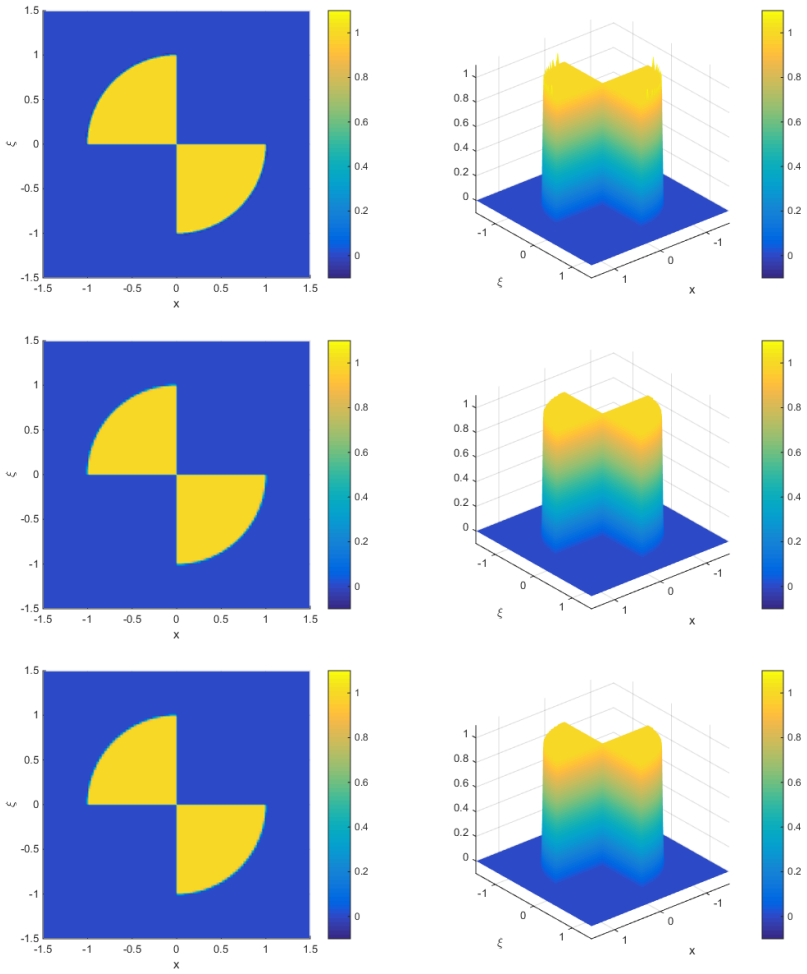

FIG. 5.1. *1D1V problem with an exact L^∞ solution in Example* 5.2. *Contour plot (left) and 3D plot (right) of the initial solution at $t = 0$ without limiter (top), initial solution after applying the TVB minmod limiter (middle), and initial solution after applying the bound-preserving limiter (bottom) on* 100×100 *meshes.*

We further measure the errors between the exact solution and the numerical solution obtained by the HPDG scheme with the bound-preserving limiter. The errors are measured outside the "pollution domain" near discontinuity, as shown in Figure 5.3(a). The L^1 errors and orders of accuracy for the HPDG method with polynomials of degree k ($k = 1, 2, 3$) are listed in Table 5.3. It can be observed that the HPDG method with P^1 and P^2 polynomials achieves the optimal second and third order of accuracy, respectively, while the convergence rate of the HPDG method with P^3 polynomials is about 3.5.

Example 5.3 (1D1V problem with a measure-valued solution). In this example, we consider one-dimensional Liouville equation (2.1) with the same potential (5.2) as in Example 5.2. The initial condition is given by

$$f(0, x, \xi) = \delta(\xi - \nu(x)), \tag{5.5}$$

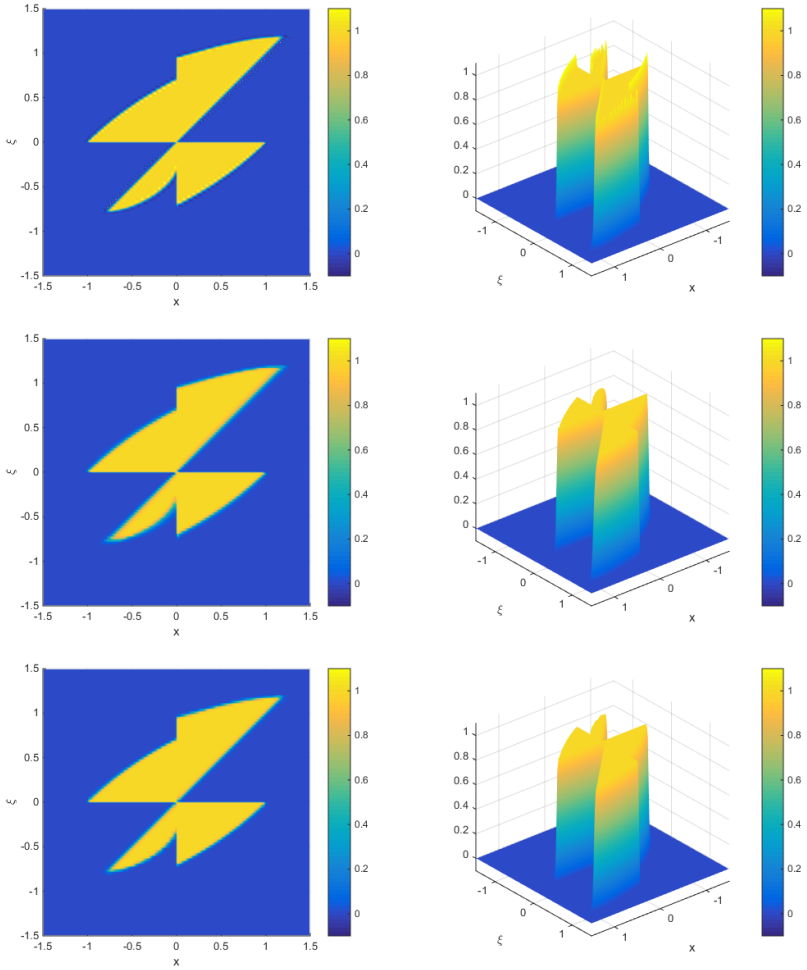

FIG. 5.2. *1D1V problem with an exact L^∞ solution in Example 5.2. Contour plot (left) and 3D plot (right) of the numerical solution of DG method without any limiter (top), numerical solution of DG method with the TVB minmod limiter (middle) and numerical solution of the proposed DG method with the bound-preserving limiter (bottom) on 100×100 meshes at $t = 1$ (with $k = 2$).*

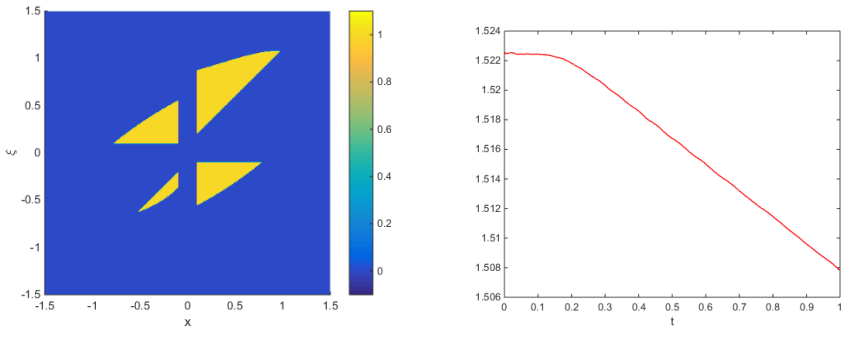

(a) Domain for accuracy test. (b) Time evolution of $\int f dxdv$

FIG. 5.3. *1D1V problem with an exact L^∞ solution in Example 5.2. (a) The domain (marked with yellow) used to measure the errors in Table 5.3. (b) Time evolution of $\int f dxd\xi$ of the HPDG method with piecewise P^2 polynomial.*

TABLE 5.3
Errors and orders of accuracy for the HPDG method solving the Liouville equation in Example 5.2.

	P^1		P^2		P^3	
$N_x \times N_\xi$	L^1 error	Order	L^1 error	Order	L^1 error	Order
20×20	8.46E-03		2.95E-03		1.63E-03	
30×30	4.00E-03	1.85	8.67E-04	3.02	3.96E-04	3.49
40×40	2.10E-03	2.24	3.64E-04	3.02	1.75E-04	2.83
50×50	1.34E-03	2.02	1.57E-04	3.76	7.79E-05	3.63

where

$$\nu(x) = \begin{cases} 0.9, & x \le -2, \\ 0.9 - \dfrac{0.9}{4}(x+2)^2, & -2 < x \le 0, \\ -0.9 + \dfrac{0.9}{4}(x-2)^2, & 0 < x < 2, \\ -0.9, & x \ge 2. \end{cases} \tag{5.6}$$

The computational domain is $[-2, 2] \times [-1.6, 1.6]$. This example is a 1D1V problem with a measure-valued solution [19], which may arise in the computation of the semiclassical limit of the Schrodinger equation. We are interested in the approximation of the moments, such as the density ρ and the averaged velocity u, defined as

$$\rho(t,x) = \int f(t,x,\xi)d\xi, \qquad u(t,x) = \frac{\int f(t,x,\xi)\xi d\xi}{\int f(t,x,\xi)d\xi}.$$

Following the level set method proposed in [18] for smooth potentials and extended in [19] to discontinuous potentials, we decompose f into the level set function f_1 and the modified density function f_2, which satisfy the same Liouville equation (2.1) with the following initial conditions:

$$f_1(0,x,\xi) = 1, \qquad f_2(0,x,\xi) = \xi - \nu(x).$$

The moments ρ and u can be numerically approximated by

$$\begin{aligned} \rho(t,x) &= \int f_1(t,x,\xi)\delta_\omega(f_2(t,x,\xi))d\xi, \\ u(t,x) &= \frac{1}{\rho(t,x)} \int f_1(t,x,\xi)\xi\delta_\omega(f_2(t,x,\xi))d\xi \end{aligned} \tag{5.7}$$

on a uniform mesh [14]. Here δ_ω is an approximation to the δ function, given by

$$\delta_\omega(x) = \begin{cases} \dfrac{1}{2\omega}(1 + \cos(|\pi x|/\omega)), & \left|\dfrac{x}{\omega}\right| \le 1, \\ 0, & \left|\dfrac{x}{\omega}\right| > 1, \end{cases} \tag{5.8}$$

and ω is taken as half of the support size of the discrete delta function δ_ω. In our computation, we take

$$\omega = \max(|(f_2)_\xi|, 1)\Delta x,$$

where the derivative $(f_2)_\xi$ can be directly computed from the polynomial expression of f_2 in each cell. The exact velocity profile and the corresponding velocity at $t = 1.8$ can be found in the appendix of [19].

We perform numerical simulations for the proposed DG method with P^2 piecewise polynomials on 400×320 meshes up to $t = 1.8$. Figure 5.4 shows the density and the averaged velocity of the exact solutions and numerical solutions at $t = 1.8$.

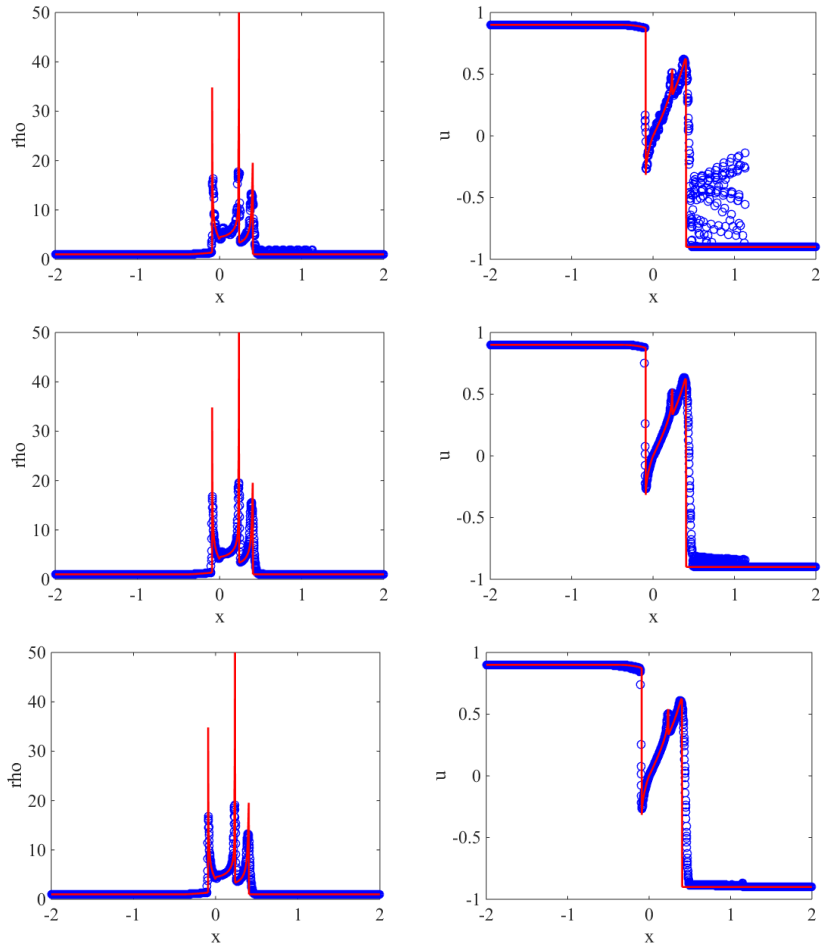

FIG. 5.4. *1D1V problem with a measure-valued solution in Example* 5.3. *Exact solution (lines) and numerical solution (circles) of the density (left) and the averaged velocity (right) of the proposed DG method at* $t = 1.8$ *with* $k = 2$ *without any limiter (top), with the TVB minmod limiter (middle), and with the bound-preserving limiter (bottom) on* 400×320 *meshes.*

The numerical solutions are obtained by the HPDG method without any limiter, by the HPDG method with the TVB minmod limiter [10], and by the HPDG method with the bound-preserving limiter to keep $-2.4 \le f_2 \le 2.4$ for the decomposed equation $f_2(x, \xi, 0) = \xi - \nu(x)$. We observe that there are oscillations for the solutions without any limiter, especially in the average velocity plot. Both limiters can achieve satisfying nonoscillatory results for the density, while the boundary-preserving limiter yields a better nonoscillatory approximation than the TVB minmod limiter for the averaged velocity, especially in the average velocity plot near the region $x \in [0.3, 1]$. In addition, we also observe that the average velocity is better resolved in this region when compared with the result in [19] obtained with the finite volume method on a much refined mesh, thanks to the high order feature of the proposed HPDG methods.

Example 5.4 (2D2V problem with a measure-valued solution). In this example, we consider the two-dimensional Liouville equation given by

$$f_t + \xi f_x + \eta f_y - V_x f_\xi - V_y f_\eta = 0, \tag{5.9}$$

with a discontinuous potential

$$V(x,y) = \begin{cases} 0.1, & x > 0, y > 0, \\ 0, & \text{else.} \end{cases} \tag{5.10}$$

The initial condition takes the form

$$f(0,x,y,\xi,\eta) = \rho(0,x,y)\delta(\xi - p(x,y))\delta(\eta - q(x,y)), \tag{5.11}$$

where

$$\rho(0,x,y) = \begin{cases} 0, & x > -0.1, y > -0.1, \\ 1, & \text{else,} \end{cases} \tag{5.12}$$

$$p(x,y) = q(x,y) = \begin{cases} 0.4, & x > 0, y > 0, \\ 0.6, & \text{else.} \end{cases} \tag{5.13}$$

The computational domain is set as $[x,y,\xi,\eta] \in [-0.2,0.2] \times [-0.2,0.2] \times [0.3,0.9] \times [0.3,0.9]$. This example is a 2D2V problem with a measure-valued solution studied in [19]. We are interested in the approximation of the zeroth moment, i.e., the density ρ, defined as

$$\rho(t,x,y) = \int\int f(t,x,y,\xi,\eta)d\xi d\eta. \tag{5.14}$$

The exact density at time $t = 0.4$ is given by

$$\rho(0.4,x,y) = \begin{cases} 1, & x < 0 \text{ or } y < 0, \\ 1.5, & 0 \le x \le \dfrac{14}{150}, \ y \ge \dfrac{3x}{2}, \\ 1.5, & 0 \le y \le \dfrac{14}{150}, \ y \le \dfrac{2x}{3}, \\ 0, & \text{otherwise.} \end{cases} \tag{5.15}$$

We perform numerical simulations of the proposed HPDG method with piecewise P^1 polynomials up to $t = 0.4$ with a positivity-preserving limiter. Figure 5.5 shows

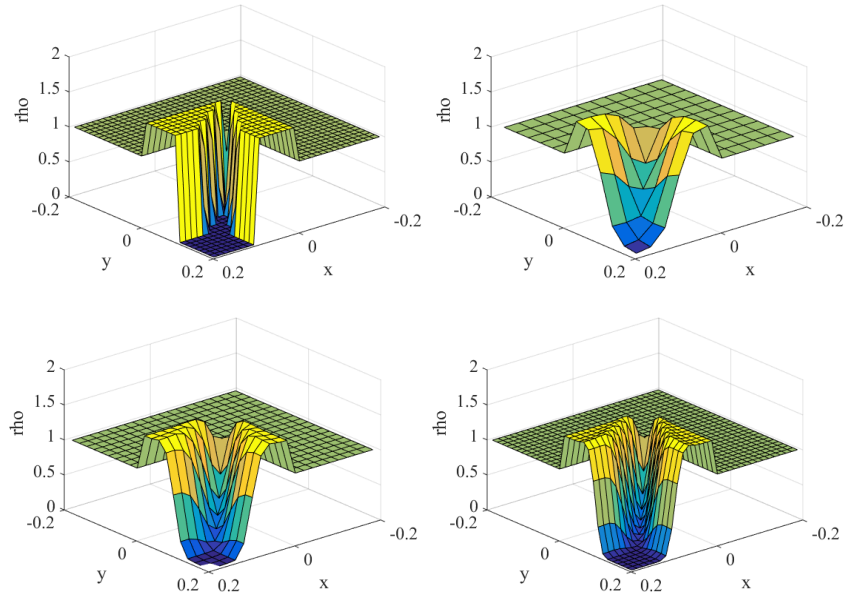

FIG. 5.5. *2D2V problem with a measure-valued solution in Example* 5.4. *Exact solution (top left) and numerical solutions of the density with* $k = 1$ *on the* 12^4 *(top right),* 20^4 *(bottom left), and* 30^4 *(bottom right) meshes at* $t = 0.4$.

numerical results of the density ρ with 12^4, 20^4, and 30^4 meshes in the phase space, compared with the reference exact solution. We can observe that, as the meshes are refined, the solution converges to the exact solution. When compared with the numerical results in [19], the proposed high order HPDG method can achieve a sharper transition near discontinuity with a coarser mesh.

6. Conclusions. In this paper, we design the HPDG method for the Liouville equation with discontinuous potentials to maintain constant Hamiltonian across a potential barrier, which allows us to capture the correct transmission and reflection behavior of particles. The proposed method can also be viewed as a high order extension of the finite difference and finite volume methods discussed in [19]. Based on the standard DG method for hyperbolic conservation laws, we make extra effort to construct numerical fluxes to take care of the behavior of a particle at a potential barrier such as either crossing it with a different momentum or being reflected. We further apply a positivity-preserving limiter to add extra robustness and stability. We provide a theoretical study of the positivity and stability properties of our proposed scheme. Numerical results show the accuracy and robustness of the proposed methods for 1D1V and 2D2V test problems. The discontinuity of the potential $V(x)$ in the 2D2V setting is assumed to occur only in the direction aligned with our spatial discretization in this paper. Future works include the generalization of the HPDG scheme to the case of curved discontinuity to further leverage the flexibility of DG method and the study of HPDG method on unstructured meshes to accommodate general computational domains.

REFERENCES

[1] L. Ambrosio, *Transport equation and Cauchy problem for BV vector fields*, Invent. Math., 2 (2004), pp. 227–260.

[2] F. Bouchut and F. James, *One-dimensional transport equations with discontinuous coefficients*, Nonlinear Anal., 32 (1998), pp. 891–933.

[3] I. Capuzzo Dolceta and B. Perthame, *On some analogy between different approaches to first order PDEs with non-smooth coefficients*, Adv. Math. Sci. Appl., 6 (1996), pp. 689–703.

[4] Y. Cheng, A. J. Christlieb, and X. Zhong, *Energy-conserving discontinuous Galerkin methods for the Vlasov–Ampère system*, J. Comput. Phys., 256 (2014), pp. 630–655.

[5] Y. Cheng, A. J. Christlieb, and X. Zhong, *Energy-conserving discontinuous Galerkin methods for the Vlasov–Maxwell system*, J. Comput. Phys., 279 (2014), pp. 145–173.

[6] Y. Cheng, I. M. Gamba, A. Majorana, and C.-W. Shu, *A brief survey of the discontinuous Galerkin method for the Boltzmann–Poisson equations*, SeMA J., 54 (2011), pp. 47–64.

[7] B. Cockburn, S. Hou and C.-W. Shu, *The Runge-Kutta local projection discontinuous Galerkin finite element method for conservation laws* IV: *The multidimensional case*, Math. Comp., 54 (1990), pp. 545–581.

[8] B. Cockburn, G. Karniadakis, and C.-W. Shu, *The development of discontinuous Galerkin methods*, in Discontinuous Galerkin Methods: Theory, Computation and Applications, B. Cockburn, G. Karniadakis, and C.-W. Shu, eds., Lect. Notes Comput. Sci. Eng., Springer, Berlin, 2000, pp. 3–50.

[9] B. Cockburn, S.-Y. Lin, and C.-W. Shu, *TVB Runge-Kutta local projection discontinuous Galerkin finite element method for conservation laws* III: *One dimensional systems*, J. Comput. Phys., 84 (1989), pp. 90–113.

[10] B. Cockburn and C.-W. Shu, *TVB Runge–Kutta local projection discontinuous Galerkin finite element method for conservation laws* II: *General framework*, Math. Comp., 52 (1989), pp. 411–411.

[11] B. Cockburn and C.-W. Shu, *Runge–Kutta discontinuous Galerkin methods for convection-dominated problems*, J. Sci. Comput., 16 (2001), pp. 173–261.

[12] R. J. DiPerna and P. L. Lions, *Ordinary differential equations, transport theory and Sobolev spaces*, Invent. Math., 98 (1989), pp. 511–547.

[13] E. Endeve, C. D. Hauck, Y. Xing, and A. Mezzacappa, *Bound-preserving discontinuous Galerkin methods for conservative phase space advection in curvilinear coordinates*, J. Comput. Phys., 287 (2015), pp. 151–183.

[14] B. Engquist, A.-K. Tornberg, and R. Tsai, *Discretization of Dirac delta functions in level set methods*, J. Comput. Phys., 207 (2005), pp. 28–51.
[15] F. Filbet and C.-W. Shu, *Discontinuous-Galerkin methods for a kinetic model of self-organized dynamics potentials*, Math. Models Methods Appl. Sci., 28 (2018), pp. 1171–1197.
[16] L. Gosse and F. James, *Numerical approximations of one-dimensional linear conservation equations with discontinuous coefficients*, Math. Comp., 69 (2000), pp. 987–1015.
[17] S. Jin and X. Liao, *A Hamiltonian-preserving scheme for high frequency elastic waves in heterogeneous media*, J. Hyperbolic Differ. Equ., 3 (2006), pp. 741–777.
[18] S. Jin, H. Liu, S. Osher, and Y.-H. R. Tsai, *Computing multivalued physical observables for the semiclassical limit of the Schrödinger equation*, J. Comput. Phys., 205 (2005), pp. 222–241.
[19] S. Jin and X. Wen, *Hamiltonian-preserving schemes for the Liouville equation with discontinuous potentials*, Commun. Math. Sci., 3 (2005), pp. 285–315.
[20] S. Jin and X. Wen, *Hamiltonian-preserving schemes for the Liouville equation of geometrical optics with discontinuous local wave speeds*, J. Comput. Phys., 214 (2006), pp. 672–697.
[21] S. Jin and X. Wen, *A Hamiltonian-preserving scheme for the Liouville equation of geometrical optics with partial transmissions and reflections*, SIAM J. Numer. Anal., 44 (2006), pp. 1801–1828.
[22] S. Jin and D. Yin, *Computational high frequency waves through curved interfaces via the Liouville equation and geometric theory of diffraction*, J. Comput. Phys., 227 (2008), pp. 6106–6139.
[23] X. Li, *l^1-error estimates for a Hamiltonian-preserving Liouville equation the Liouville equation with piecewise constant potentials: A simple proof*, J. Comput. Math., 35 (2017), pp. 814–827.
[24] X. Liu and S. Osher, *Nonoscillatory high order accurate self-similar maximum principle satisfying shock capturing schemes* I, SIAM J. Numer. Anal., 33 (1996), pp. 760–779.
[25] B. Perthame and C.-W. Shu, *On positivity preserving finite volume schemes for Euler equations*, Numer. Math., 73 (1996), pp. 119–130.
[26] B. Perthame and C. Simeoni, *A kinetic scheme for the Saint-Venant system with a source term*, Calcolo, 38 (2001), pp. 201–231.
[27] G. Petrova and B. Popov, *Linear transport equations with discontinuous coefficients*, J. Math. Anal. Appl., 260 (2001), pp. 307–324.
[28] F. Poupaud and M. Rascle, *Measure solutions to the linear multidimensional transport equation with non-smooth coefficients*, Comm. Partial Differential Equations, 22 (1997), pp. 337–358.
[29] J.-M. Qiu and C.-W. Shu, *Positivity preserving semi-Lagrangian discontinuous Galerkin formulation: Theoretical analysis and application to the Vlasov-Poisson system*, J. Comput. Phys., 230 (2011), pp. 8386–8409.
[30] W. H. Reed and T. Hill, *Triangular Mesh Methods for the Neutron Transport Equation*, technical report, Los Alamos Scientific Lab, 1973.
[31] C.-W. Shu and S. Osher, *Efficient implementation of essentially non-oscillatory shock-capturing schemes*, J. Comput. Phys., 77 (1988), pp. 439–471.
[32] J. Staudacher and E. Savin, *Conservative finite-difference scheme for high-frequency acoustic waves propagating at an interface between two media*, Commun. Comput. Phys, 11 (2012), pp. 351–366.
[33] X. Wen, *The L^1-error estimates for a Hamiltonian-preserving Liouville equation the Liouville equation with piecewise constant potentials and perturbed initial data*, J. Comput. Math., 29 (2010), pp. 1–23.
[34] X. Wen and S. Jin, *The L^1-error estimates for a Hamiltonian-preserving scheme for the Liouville equation with piecewise constant potentials*, SIAM J. Numer. Anal., 46 (2008), pp. 2688–2714.
[35] X. Wen and S. Jin, *The L^1-stability of a Hamiltonian-preserving scheme for the Liouville equation with discontinuous potentials*, J. Comput. Math., 27 (2009), pp. 45–67.
[36] X. Zhang and C.-W. Shu, *Maximum-principle-satisfying and positivity-preserving high-order schemes for conservation laws: Survey and new developments*, Proc. A, 467 (2011), pp. 2752–2776.
[37] X. Zhang and C. Shu, *On positivity preserving high order discontinuous Galerkin schemes for compressible Euler equations on rectangular meshes*, J. Comput. Phys., 328 (2017), pp. 301–343.